

Highlights

HOG-CNN: Integrating Histogram of Oriented Gradients with Convolutional Neural Networks for Retinal Image Classification

Faisal Ahmed

- We propose a novel HOG-CNN framework that integrates Histogram of Oriented Gradients (HOG) with deep CNN features for retinal disease diagnosis.
- Our model demonstrates state-of-the-art performance in disease classification tasks, achieving up to 98.5% accuracy and an AUC of 99.2 for diabetic retinopathy (DR) classification on the AP-TOS dataset, and up to 92.8% accuracy, precision 94.8%, and an AUC of 94.5 for age-related macular degeneration (AMD) classification on the IC-Dataset.
- HOG-CNN demonstrates strong generalization across three retinal diseases—AMD, DR, and Glaucoma—using multiple public benchmark datasets.
- The hybrid design effectively captures both local texture patterns and high-level semantic information from fundus images.
- Our model offers a lightweight and interpretable alternative to complex deep learning systems, making it suitable for real-world, resource-constrained clinical environments.

HOG-CNN: Integrating Histogram of Oriented Gradients with Convolutional Neural Networks for Retinal Image Classification

Faisal Ahmed^{a,*}

^aDepartment of Data Science and Mathematics, Embry-Riddle Aeronautical University, 3700 Willow Creek Rd, Prescott, Arizona 86301, USA

Abstract

The analysis of fundus images is critical for the early detection and diagnosis of retinal diseases such as Diabetic Retinopathy (DR), Glaucoma, and Age-related Macular Degeneration (AMD). Traditional diagnostic workflows, however, often depend on manual interpretation and are both time- and resource-intensive. To address these limitations, we propose an automated and interpretable clinical decision support framework based on a hybrid feature extraction model called *HOG-CNN*.

Our key contribution lies in the integration of handcrafted Histogram of Oriented Gradients (HOG) features with deep convolutional neural network (CNN) representations. This fusion enables our model to capture both local texture patterns and high-level semantic features from retinal fundus images. We evaluated our model on three public benchmark datasets: APTOS 2019 (for binary and multiclass DR classification), ORIGA (for Glaucoma detection), and IC-AMD (for AMD diagnosis); HOG-CNN demonstrates consistently high performance. It achieves **98.5% accuracy and 99.2 AUC** for binary DR classification, and **94.2 AUC** for five-class DR classification. On the IC-AMD dataset, it attains **92.8% accuracy, 94.8% precision and 94.5 AUC**, outperforming several state-of-the-art models. For Glaucoma detection on ORIGA, our model achieves **83.9% accuracy and 87.2 AUC**, showing competitive performance despite dataset limitations.

We show, through comprehensive appendix studies, the complementary strength of combining HOG and CNN features. The model's lightweight and interpretable design makes it particularly suitable for deployment in resource-constrained clinical environments. These results position HOG-CNN as a robust and scalable tool for automated retinal disease screening.

Keywords: Retinal Disease Diagnosis, Histogram of Oriented Gradients, Deep Learning, Ophthalmology.

1. Introduction

As of August 2023, the World Health Organization (WHO) reports that over 2.2 billion people globally experience near or distance vision impairment, with at least 1 billion cases being preventable or yet to be addressed. Among the leading causes of vision impairment and blindness are glaucoma, diabetic retinopathy (DR), and age-related macular degeneration (AMD). Specifically, the WHO estimates that glaucoma affects 7.7 million, DR affects 3.9 million, and AMD affects 8 million individuals worldwide. [1]. These figures underscore the significant global burden of serious eye diseases, highlighting the need for improved access to eye care services worldwide. As most patients with eye

diseases are not aware of the aggravation of these conditions, early screening and treatment of eye diseases are quite important. Currently, detecting these conditions is a time-consuming and manual process that requires a trained clinician to examine and evaluate digital color fundus images of the retina, which can result in delayed treatment. Therefore, the need for clinical decision-support methods has long been recognized. Recent advancements have further enhanced diagnostic capabilities, particularly in predicting disease progression. For example, an automated ML model has been shown to effectively predict short-term DR progression using ultra-widefield retinal images, with promising implications for early screening and improved vision outcomes [2]. Additionally, deep learning algorithms have demonstrated strong performance in forecasting the progression to geographic atrophy in AMD patients by an-

*Corresponding author

Email address: ahmedf9@erau.edu (Faisal Ahmed)

alyzing spectral-domain optical coherence tomography images. Integrating clinical data with optical coherence tomography angiography has also led to improvements in DR classification accuracy [3]. Despite these advancements, current ML methods often lack computational efficiency when applied to large datasets and remain limited in interpretability, which is crucial for providing actionable insights to ophthalmologists. To address these limitations, recent approaches such as HOG-CNN leverage histograms of oriented gradients to enhance both the performance and interpretability of retinal image analysis models.

Driven by this motivation, the past decade has seen extensive use of machine learning (ML) techniques in the analysis of retinal images [4, 5]. Significant advancements have been achieved through approaches such as image classification and pattern recognition [6]. The emergence and success of convolutional neural networks (CNNs) in image classification further demonstrated the effectiveness of ML in retinal image processing [7]. Despite these advances, many of these methods fall short in terms of computational efficiency for handling large-scale datasets and lack the interpretability needed to support ophthalmologists in diagnosing diseases.

In this study, we propose a novel hybrid approach for retinal disease classification by incorporating Histogram of Oriented Gradients (HOG) features into deep learning models. Inspired by the foundational work of Dalal and Triggs [8], where HOG descriptors were effectively utilized for human detection, we extend this technique to the domain of retinal image analysis. Specifically, we extract HOG features from each retinal fundus image, resulting in a high-dimensional descriptor of size 26,244 per image. These handcrafted features are then fused with deep features obtained from a pre-trained convolutional neural network (CNN), forming a hybrid HOG-CNN architecture. The integration of structural gradient information with learned visual representations enhances the model’s ability to discriminate between disease categories. Experimental results of our model HOG-CNN demonstrate that the proposed HOG-CNN model achieves superior performance compared to conventional CNN-based classifiers, highlighting the benefits of combining traditional feature engineering with modern deep learning techniques.

Our contributions.

- We propose a novel HOG-CNN framework that integrates Histogram of Oriented Gradients (HOG) with deep CNN features for retinal disease diagnosis.

- Our model demonstrates state-of-the-art performance in disease classification tasks, achieving up to 98.5% accuracy and an AUC of 99.2 for diabetic retinopathy (DR) classification on the AP-TOS dataset, and up to 92.8% accuracy, precision 94.8% and an AUC of 94.5 for age-related macular degeneration (AMD) classification on the IC-Dataset.
- HOG-CNN demonstrates strong generalization across three retinal diseases—AMD, DR, and Glaucoma—using multiple public benchmark datasets.
- The hybrid design effectively captures both local texture patterns and high-level semantic information from fundus images.
- Our model offers a lightweight and interpretable alternative to complex deep learning systems, making it suitable for real-world, resource-constrained clinical environments.

2. Related Work

In the past decade, machine learning (ML) tools have been extensively employed in medical image analysis [9, 10]. In particular, within the domain of retinal image analysis, ML methodologies have demonstrated significant effectiveness [7]. There are two primary applications of ML in retinal imaging: (1) the diagnosis and grading of diseases, which is typically framed as a classification problem for image data [11], and (2) lesion detection and segmentation [4]. In this paper, we focus exclusively on the diagnosis and grading of retinal diseases by leveraging and integrating Histogram of Oriented Gradients (HOG) features with pre-trained convolutional neural network (CNN) models.

Topological Data Analysis (TDA) is an emerging approach that is increasingly being utilized in medical image analysis, including applications in retinal imaging [12, 13, 14]. Over the past decade, TDA has shown great promise across diverse fields such as image analysis, neurology, cardiology, hepatology, gene-level and single-cell transcriptomics, drug discovery, evolutionary biology, and protein structure analysis. Its strength lies in revealing latent patterns within data, offering new avenues for tasks like image segmentation, object recognition, registration, and reconstruction. In medical imaging, persistent homology (PH)—a key method in TDA—has proven effective in analyzing histopathology

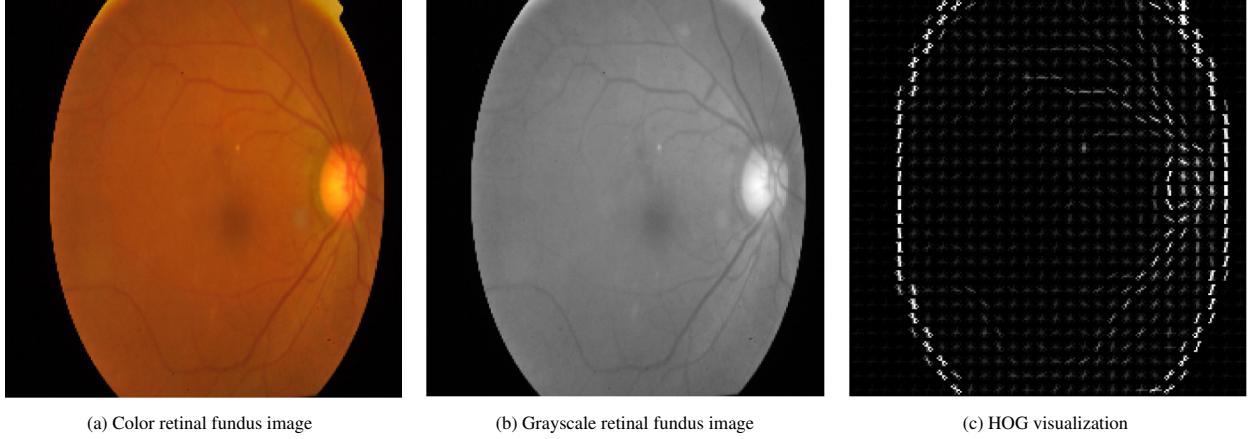


Figure 1: Illustration of the preprocessing pipeline applied to a fundus image. From left to right: (a) Original color image, (b) grayscale conversion used for HOG computation, and (c) corresponding Histogram of Oriented Gradients (HOG) visualization highlighting edge and texture features.

slides [15, 16, 17], fibrin network structures [18], tumor classification [19, 20], chest X-ray screening [21], neuronal morphology studies [22], brain artery mapping [23], fMRI analysis [24, 25], and genomic inference [26].

Following the success of CNNs in image classification tasks, deep learning methods have proven to be highly effective in retinal image analysis [5, 27]. A substantial body of literature exists on deep learning applications in ophthalmology, with comprehensive reviews available in survey papers [28, 29, 6, 4]. Moreover, recent studies have explored advanced ML models for predicting disease progression [2], and have integrated clinical data with imaging modalities such as OCT-A to improve diabetic retinopathy (DR) classification [3]. Additional reviews highlighting the current state of deep learning in ophthalmology can be found in the following works [30, 31, 32].

3. Methodology

In this study, we employ the Histogram of Oriented Gradients (HOG) technique as an effective feature extraction method for the classification of retinal images. The methodology consists of two primary stages: (1) extraction of HOG features from retinal images, and (2) integration of these features with the weights of pre-trained convolutional neural network (CNN) models to form a hybrid deep learning framework for classification. First, HOG descriptors are computed for each retinal image, capturing edge and gradient structure that are characteristic of various retinal conditions. These descriptors are then used to augment the feature representations learned by the CNN models. By combin-

ing handcrafted features with deep features, we aim to enhance the discriminative power of the model. In the subsequent subsections, we detail the process of HOG feature extraction and the integration strategy used to combine these features with the pre-trained CNNs.

3.1. HOG Feature Extraction from Retinal Images

In this study, we employed the Histogram of Oriented Gradients (HOG) as a feature extraction technique to capture the texture and structural characteristics of retinal fundus images. HOG is a widely-used descriptor for object detection and image classification due to its ability to encode gradient orientation distributions, which are particularly useful in representing local shape and edge information.

The feature extraction pipeline began with data acquisition, denoted as $\mathcal{I} = \{I_1, I_2, \dots, I_n\}$, where each I_k represents a color fundus image. Each image was resized to a uniform spatial resolution of 224×224 pixels to ensure consistency across the dataset and to facilitate compatibility with pre-trained convolutional neural network (CNN) models used later in our hybrid framework. This resizing can be denoted as:

$$I'_k = \text{Resize}(I_k, 224 \times 224)$$

Following resizing, each RGB image I'_k was converted to a grayscale image G_k using a luminance-preserving transformation:

$$G_k(x, y) = 0.299 \cdot R(x, y) + 0.587 \cdot G(x, y) + 0.114 \cdot B(x, y)$$

This grayscale conversion is essential since HOG operates on intensity gradients, and color information does not significantly enhance gradient-based descriptors.

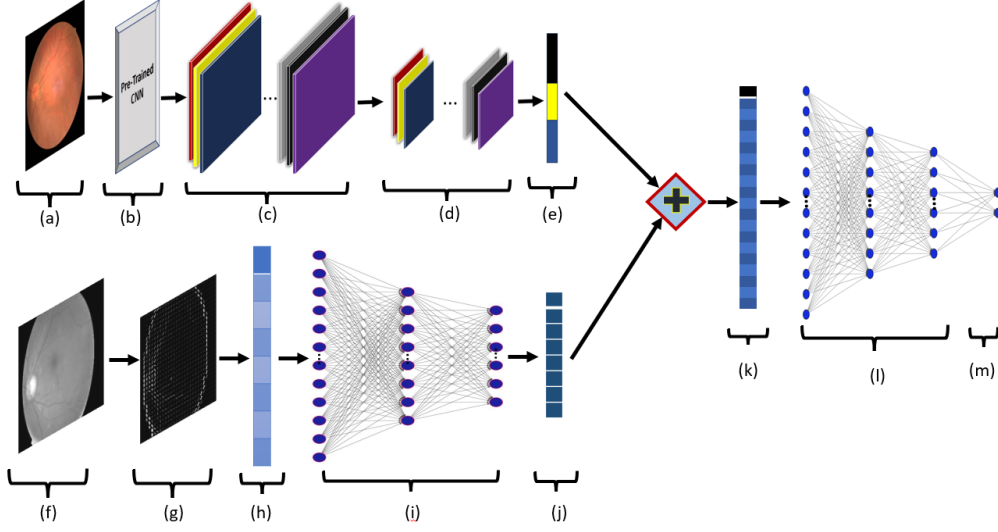


Figure 2: **Overview of the proposed model HOG-CNN architecture:** The model accepts two inputs: (a) a color fundus image and (f) a grayscale fundus image. The top pathway processes (a) through (b) a pre-trained CNN, (c) a 64-filter convolutional layer, (d) a 2×2 max-pooling layer, and (e) a flattening layer. In the bottom pathway, (g) the HOG visualization is extracted from (f), and (h) its feature vector is passed through (i) a feed-forward neural network with three hidden layers of sizes 800, 256, and 128. Outputs from both pathways, (e) and (j), are concatenated to form (k), (l) which is input to a second feed-forward network with hidden layers of sizes 256 and 128, along with a dropout layer (dropout rate = 0.2). The final output layer (m) has size 2 for binary or size 5 for multi-class classification.

Once converted, the HOG descriptor was computed on each grayscale image. This involved calculating the gradient magnitude and orientation at each pixel using discrete derivative masks. The image was then partitioned into small spatial regions known as *cells*, each of size 8×8 pixels. Within each cell, a histogram of gradient directions was computed using 9 orientation bins (covering 0° to 180°). These histograms describe the distribution of edge directions within the local area.

To account for changes in illumination and contrast, these local histograms were grouped into overlapping *blocks* of 2×2 cells. Each block's histograms were concatenated and normalized using the L2-Hys norm to produce a robust local feature vector. Mathematically, this can be expressed as:

$$F_k = \text{HOG}(G_k; o = 9, p = 8 \times 8, b = 2 \times 2)$$

where $F_k \in \mathbb{R}^d$ is the resulting high-dimensional HOG descriptor for image k , and d denotes the length of the flattened feature vector. The value of d depends on the total number of cells and blocks given the fixed image resolution. In our experiment, $d = 26,244$, so $F_k \in \mathbb{R}^{26,244}$; that is, from each grayscale image, we extract a 26,244-dimensional vector.

This process was repeated for all n images in the

dataset, resulting in a feature matrix:

$$\mathbf{F} = \begin{bmatrix} F_1 \\ F_2 \\ \vdots \\ F_n \end{bmatrix} \in \mathbb{R}^{n \times d}$$

The matrix \mathbf{F} was then stored in tabular format using a DataFrame structure and exported as a CSV file named `hog_features.csv`. This stored feature set served as a structured and compressed representation of the input images, which was later used for integration with deep learning models in the classification pipeline.

Overall, this HOG-based feature extraction step aimed to leverage handcrafted descriptors that capture geometrical and textural cues in retinal images, providing a complementary signal to the abstract features learned by convolutional layers in deep neural networks.

3.2. Hybrid HOG-CNN Model

The following section outlines the methodology for combining handcrafted gradient-based features with deep convolutional features to construct a hybrid classification model for retinal image analysis. This dual-branch framework is designed to support both binary and multi-class image classification tasks, effectively

integrating traditional HOG descriptors with modern CNN-based feature representations.

In the preprocessing stage, each fundus image is formatted as a 3D tensor $\mathbf{I}_{\text{raw}} \in \mathbb{R}^{H \times W \times C}$, where H and W represent the image height and width, and $C = 3$ corresponds to the RGB color channels. No normalization is applied to pixel intensities; hence, the image tensor is passed directly into the model as:

$$\mathbf{I}_{\text{input}} = \mathbf{I}_{\text{raw}}.$$

All images are resized to a fixed dimension of (224×224) and grouped into batches of size B , represented as:

$$\mathbf{X} = \{\mathbf{I}_1, \mathbf{I}_2, \dots, \mathbf{I}_B\}, \quad \mathbf{y} = [y_1, y_2, \dots, y_B],$$

where \mathbf{y} contains the ground-truth labels for classification.

In parallel with the RGB image input stream, each fundus image is converted to grayscale and processed using the Histogram of Oriented Gradients (HOG) algorithm to extract structural edge and texture information. This results in a HOG feature vector $\mathbf{H}_i \in \mathbb{R}^d$ for each image, where d is the dimensionality of the HOG descriptor. These descriptors are passed through a three-layer fully connected neural network for dimensionality reduction and transformation. The first dense layer contains 800 ReLU-activated units, the second dense layer contains 256 ReLU-activated units, and the second contains 128 ReLU-activated units, yielding a HOG embedding vector:

$$\mathbf{F}_{\text{HOG}} = \text{ReLU}(\mathbf{W}_2 \cdot \text{ReLU}(\mathbf{W}_1 \cdot \mathbf{H} + \mathbf{b}_1) + \mathbf{b}_2).$$

Simultaneously, the RGB image \mathbf{I}_i is input into a pre-trained convolutional neural network (CNN) such as ResNet-50 or EfficientNet. The classification head of the pre-trained model is removed by setting `include_top = False`, and the convolutional base is frozen to preserve previously learned visual representations. The extracted feature maps are further processed by a 2D convolutional layer with 64 filters of size (3×3) and ReLU activation, followed by a max pooling layer with a (2×2) window. The output is then flattened and passed through a dense layer with 64 ReLU-activated units to produce the image-based embedding:

$$\mathbf{F}_{\text{CNN}} \in \mathbb{R}^{64}.$$

The two feature vectors \mathbf{F}_{CNN} and \mathbf{F}_{HOG} are concatenated to form a unified representation:

$$\mathbf{F}_{\text{concat}} = [\mathbf{F}_{\text{CNN}}, \mathbf{F}_{\text{HOG}}] \in \mathbb{R}^{192}.$$

This combined feature vector is then passed through two fully connected layers with 256 and 128 ReLU-activated units, respectively. A dropout layer with a dropout rate of $p = 0.2$ is applied to prevent overfitting. The final classification layer adapts to the task type. For binary classification, the output is computed using a sigmoid activation:

$$\hat{y} = \text{Sigmoid}(\mathbf{W}_{\text{out}} \cdot \mathbf{F}_{\text{concat}} + \mathbf{b}_{\text{out}}),$$

while for multi-class classification, a softmax activation is used:

$$\hat{\mathbf{y}} = \text{Softmax}(\mathbf{W}_{\text{out}} \cdot \mathbf{F}_{\text{concat}} + \mathbf{b}_{\text{out}}).$$

The model is trained to minimize the categorical cross-entropy loss:

$$\mathcal{L} = -\frac{1}{B} \sum_{i=1}^B \sum_{c=1}^C y_{i,c} \log(\hat{y}_{i,c}),$$

where B is the batch size and C is the number of output classes. Optimization is performed using the Adam optimizer. The model parameters θ are updated at each iteration according to:

$$\theta_{t+1} = \theta_t - \eta \cdot \nabla_{\theta} \mathcal{L},$$

where η is the learning rate.

During inference, the predicted label for each image is determined by selecting the class with the highest predicted probability:

$$\hat{y}_i = \arg \max_c \hat{y}_{i,c}.$$

To evaluate the model, standard metrics are employed. These include **accuracy**, which reflects the proportion of correct predictions, **precision**, which measures the reliability of positive predictions, **recall** or sensitivity, which assesses how well actual positives are identified, and the **F1-score**, which balances precision and recall. Additionally, the **AUC** (Area Under the Receiver Operating Characteristic Curve) is used to evaluate the model's discriminative capability. All experiments are conducted using TensorFlow/Keras with CPU acceleration, with training performed over 50 epochs and a batch size of 32. The proposed HOG-CNN model demonstrates how combining engineered features with learned deep features can yield robust classification performance, especially in medical image analysis where both texture and contextual cues are important. The HOG-CNN architecture is visually illustrated in Figure 2, and the complete algorithmic steps are summarized in here 1.



(a) Training vs. Test Accuracy (Binary Classification)



(b) Training vs. Test Loss (Binary Classification)

Figure 3: Training and Testing Accuracy and Loss over 50 Epochs on the APTOS Dataset (Binary Classification).

4. Experiments

4.1. Datasets

To see the performance of our Hog-ML model for Glaucoma, DR, and AMD screening, we did several experiments on well-known benchmark datasets. We give the basic details of these datasets in Table 1. Further details (resolution, camera, etc.) for all the datasets can be found in [4].

ICChallenge-AMD dataset is designed for the Automatic Detection challenge on Age-related Macular degeneration (ADAM Challenge) which was held as a satellite event of the ISBI 2020 conference [33, 34]. There are two different resolutions of images, i.e., 2124×2056 pixels (824 images) and 1444×1444 (376 images). While the dataset has 1200 images, only 400 of them are available with labels. Like most other references, we used these 400 images in our experiments Table 2. Among these 400 images, 89 of them are labeled as AMD, and the remaining 311 images are labeled as healthy.

ORIGA dataset contains 650 high resolution (3072×2048) retinal images for Glaucoma annotated by trained professionals from Singapore Eye Research Institute [35]. Out of 650 fundus images, 168 images are labeled as Glaucoma and the remaining 482 images are labeled as healthy.

APTOS 2019 dataset was used for a Kaggle competition on DR diagnosis [36]. The images have varying resolutions, ranging from 474×358 to 3388×2588 . APTOS stands for Asia Pacific Tele-Ophthalmology Society, and the dataset was provided by Aravind Eye Hospital in India. In this dataset, fundus images are graded

manually on a scale of 0 to 4 (0: no DR; 1: mild; 2: moderate; 3: severe; and 4: proliferative DR) to indicate different severity levels. The number of images in these classes are respectively 1805, 370, 999, 193, and 295. In the binary setting, class 0 is defined as the normal group, and the remaining classes (1-4) are defined as DR group which gives a split 1805:1857. The total number of training and test samples in the dataset were 3662 and 1928 respectively. However, the labels for the test samples were not released after the competition, so like other references, we used the available 3662 fundus images with labels. We report our results on a binary and 5-class classification setting. In a binary setting, fundus images with grades 1, 2, 3, and 4 are identified as DR group, and grade 0 images as the normal group.

4.2. Experimental Setup

Training-Test Split: Since none of the datasets provide a predefined *train:test* split, prior works have adopted varying strategies for data partitioning. To ensure fair comparison, we follow the most commonly used splits reported in the literature. Specifically, for the APTOS dataset (both binary and 5-class tasks) and the ORIGA dataset, we adopt an 80:20 training-to-testing ratio for evaluating our HOG-CNN model. For the ICChallenge-AMD dataset, we employ 5-fold cross-validation and report the mean performance across all folds.

Because of the discrepancy between the experimental setups of different methods, we give the train:test splits of all models in our accuracy tables to facilitate a fair comparison (Tables 2 to 5).

No Data Augmentation: Note that as our datasets are

Algorithm 1: Training Procedure for Hybrid HOG-CNN Model

Input: Fundus image dataset $\mathcal{D} = \{(\mathbf{I}_i, y_i)\}_{i=1}^N$,
classification type (binary or multi-class),
number of epochs E

Output: Trained HOG-CNN model and
evaluation metrics

Step 1: HOG Feature Extraction

for $i \leftarrow 1$ **to** N **do**

 Convert \mathbf{I}_i to grayscale
 Extract HOG descriptor $\mathbf{H}_i \in \mathbb{R}^d$
 Pass \mathbf{H}_i through Dense(800, ReLU) \rightarrow
 Dense(256, ReLU) \rightarrow Dense(128, ReLU)
 to obtain HOG embedding \mathbf{F}_{HOG}

Step 2: CNN Feature Extraction

for $i \leftarrow 1$ **to** N **do**

 Resize \mathbf{I}_i to (224, 224, 3) without
 normalization
 Pass \mathbf{I}_i through pre-trained CNN backbone
 (with frozen weights,
 include_top=False)
 Apply Conv2D(64 filters, 3×3 , ReLU),
 MaxPooling(2×2), Flatten, Dense(64,
 ReLU) to obtain CNN embedding \mathbf{F}_{CNN}

Step 3: Feature Fusion and Classification

for $i \leftarrow 1$ **to** N **do**

 Concatenate \mathbf{F}_{CNN} and \mathbf{F}_{HOG} to get
 $\mathbf{F}_{\text{concat}} \in \mathbb{R}^{192}$
 Pass $\mathbf{F}_{\text{concat}}$ through Dense(256, ReLU) \rightarrow
 Dense(128, ReLU) \rightarrow Dropout(0.2)
 Apply output layer with Sigmoid (binary) or
 Softmax (multi-class) activation to get
 predictions \hat{y}

Train the model over 50 epochs minimizing
categorical cross-entropy loss using Adam
optimizer; evaluate with Accuracy, Precision,
Recall, F1-score, AUC metrics.

return Trained HOG-CNN model and evaluation
metrics

quite small and imbalanced compared to other image classification tasks for deep learning models, hence all CNN and other deep learning methods need to use serious data augmentation (sometimes 50-100 times) to train their model and avoid overfitting [37]. We do not use any type of data augmentation or pre-processing to increase the size of training data for HOG-CNN model. This makes our model computationally very efficient. We used the original datasets and did not use any kind of data augmentation as we used pre-trained models as backbone.

HOG-CNN Model Hyperparameters: We extracted 26,244 HOG features per image. Then we integrated these features with pre-trained CNN features. We trained the HOG-CNN model for 50 epochs using a batch size of 32 for all datasets. We used the Adam optimizer and kept the remaining parameters as default. To reduce overfitting, we incorporated a Dropout layer with a rate of 0.2 and employed early stopping with a patience of 10, restoring the best-performing model weights for final prediction.

Our code is available at the following link ¹.

5. Results

AMD Detection Results: Table 2 presents the classification performance of recent methods on the *ICChallenge-AMD* dataset. Our proposed HOG-CNN attains the highest overall accuracy of 92.8%, surpassing the previous best DCNN (91.7%) and edging out the self-supervised S2C2L (92.5%). HOG-CNN also records the best precision (94.8%), indicating a notably low false-positive rate. Conversely, S2C2L achieves the top recall (82.4%) and the highest AUC (97.5%), showing stronger sensitivity but slightly lower specificity than our model. Other self-supervised approaches—including Rotation S (87.6% Acc), Invariant (86.6% Acc), and Mem-Bank, Decouple, and Contrastive (all $\leq 83.8\%$ Acc)—trail behind both HOG-CNN and S2C2L. These results demonstrate that integrating handcrafted HOG descriptors with deep CNN

¹<https://github.com/FaisalAhmed77/HOG-CNN>

Table 1: Benchmark datasets for fundus images.

Dataset	Disease	Total	Normal	Abnormal
APTOS 2019	DR	3662	1805	1857
ORIGA	GI	650	482	168
ICChallenge-AMD	AMD	400	311	89

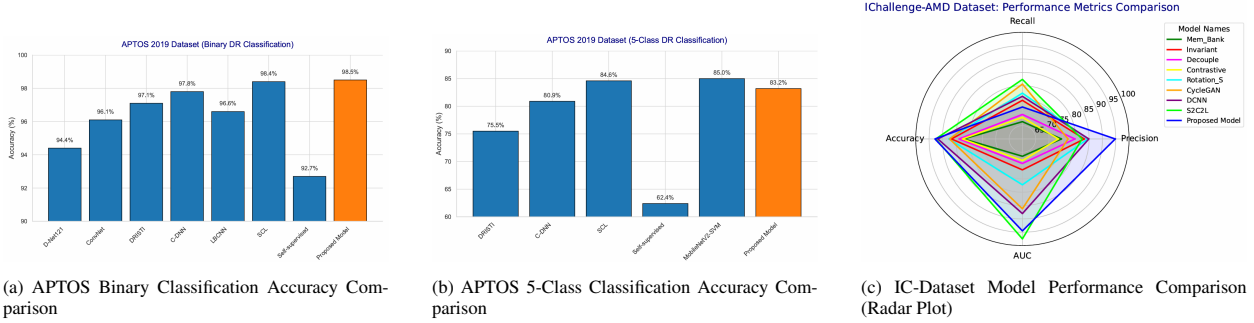


Figure 4: Accuracy comparison of the proposed model with existing deep learning methods: (a) and (b) show bar plots for binary and 5-class classification on the APTOS 2019 dataset, respectively; (c) presents a radar chart comparing multiple metrics on the IC-Dataset.

representations yields more discriminative features, delivering superior AMD detection accuracy compared with existing purely CNN-based or self-supervised techniques.

DR Detection Results: We report diabetic retinopathy (DR) detection results using the APTOS 2019 dataset under both binary and multiclass classification settings, as presented in Table 3 and Table 4, respectively. In the binary classification setting (Table 3), our proposed HOG-CNN model achieved the best overall performance, obtaining a precision, recall, and accuracy of 98.5%, along with an AUC of 99.2%. This outperforms several state-of-the-art models, including SCL [38] (98.4% accuracy, 98.9% AUC), C-DNN [39] (97.8% accuracy), and LBCNN [40] (96.6% accuracy, 98.7% AUC). Notably, our method surpasses these models in all reported metrics, indicating superior diagnostic capability and a stronger balance between sensitivity and specificity.

In the more challenging multiclass classification setting (Table 4), which involves classifying DR into five severity levels, the HOG-CNN model continued to demonstrate competitive performance. It achieved a precision of 86.0%, recall of 78.6%, accuracy of 83.2%, and the highest AUC of 94.2% among all compared methods. While MobileNetV2-SVM [41] slightly outperformed in terms of accuracy (85.0%) and recall (74.8%), our model offered the best precision and AUC, making it more reliable for nuanced multiclass predictions. Other approaches, such as SCL [38] (84.6% accuracy, 93.8% AUC) and C-DNN [39] (80.9% accuracy), lagged behind in overall metrics.

These results demonstrate that the proposed integration of handcrafted HOG features with deep CNN representations enhances the model’s ability to capture both local texture variations and high-level semantic features, leading to superior performance in both binary and mul-

ticlass DR diagnosis tasks. The consistently high AUC scores also suggest that our HOG-CNN model maintains strong discriminative power across different DR severity levels, making it a promising tool for real-world clinical applications.

Glaucoma Detection Results: We evaluate the performance of our HOG-CNN model for glaucoma diagnosis using the ORIGA dataset, as summarized in Table 5. The proposed model achieved an accuracy of 83.9%, sensitivity of 83.9%, specificity of 82.0%, and an AUC of 87.2%. Although the performance does not surpass the top-performing models such as CAD [42] (96.5% accuracy, 98.1% sensitivity, 94.2% AUC) and ODGNet [43] (95.8% accuracy, 94.8% sensitivity, 97.9% AUC), our model still shows solid results given its simplicity and lack of domain-specific pretraining or segmentation-based preprocessing.

In contrast to methods like EAMNet [44] and 18-CNN [45], which either did not report full performance metrics or underperformed in terms of sensitivity (e.g., 58.1% for 18-CNN), our HOG-CNN model strikes a better balance between sensitivity and specificity. It also compares competitively to SVM-SMOTE [46], which achieved 82.8% accuracy and 88.9 AUC, slightly lower than our AUC of 87.2.

While ensemble or segmentation-based models like CAD [42], ODGNet [43], and CNN-SVM [47] achieve superior performance, they typically rely on complex pipelines, including optic disc segmentation or pre-trained architectures. In contrast, our model integrates handcrafted HOG features with CNN-based representations in a lightweight and efficient framework. These findings support the utility of the HOG-CNN model as a viable and generalizable approach, especially in scenarios with limited computational resources or where interpretability of feature representations is important.

Table 2: Accuracy results for AMD diagnosis.

IChallenge-AMD Dataset							
Method	Nor:Abn	Train:Test	Class	Prec	Recall	Acc	AUC
Mem-Bank [48]	311:89	5 fold CV	2	74.6	66.5	82.0	66.5
Invariant [49]	311:89	5 fold CV	2	83.2	74.5	86.6	71.6
Decouple [50]	311:89	5 fold CV	2	79.7	69.2	83.8	69.2
Contrastive [51]	311:89	5 fold CV	2	73.5	68.1	82.5	68.1
Rotation S [52]	311:89	5 fold CV	2	84.5	77.2	87.6	77.2
CycleGAN [53]	933:267	5 fold CV	2	77.1	80.6	87.3	86.2
DCNN [54]	311:89	10 fold CV	2	84.9	76.0	91.7	88.0
S2C2L [55]	311:89	5 fold CV	2	82.35	82.35	<u>92.50</u>	97.5
HOG-CNN	311:89	5 fold CV	2	94.8	72.0	92.8	<u>94.5</u>

Table 3: Accuracy results for binary DR diagnosis.

APTOS 2019 Dataset Binary (DR)							
Method	Nor:Abn	Train:Test	Class	Prec	Recall	Acc	AUC
D-Net121 [56]	1805:1857	85:15	2	86.0	87.0	94.4	-
ConvNet [57]	1805:1857	80:20	2	-	-	96.1	-
DRISTI [58]	1805:1857	85:15	2	-	-	97.1	-
C-DNN [39]	1805:1857	85:15	2	98.0	98.0	97.8	-
LBCNN [40]	1805:1857	80:20	2	-	-	96.6	98.7
SCL [38]	1805:1857	85:15	2	<u>98.4</u>	<u>98.4</u>	<u>98.4</u>	<u>98.9</u>
Self-supervised [59]	1805:1857	10 fold	2	-	-	92.7	-
HOG-CNN	1805:1857	80:20	2	98.5	98.5	98.5	99.2

Table 4: Accuracy results for multiclass DR diagnosis.

APTOS 2019 Dataset - 5-class (DR)							
Method	Nor:Abn	Train:Test	Class	Prec	Rec	Acc	AUC
DRISTI [58]	1805:1857	85:15	5	59.4	54.6	75.5	-
C-DNN [39]	1805:1857	85:15	5	-	-	80.9	-
SCL [38]	1805:1857	85:15	5	<u>73.8</u>	70.50	<u>84.6</u>	<u>93.8</u>
Self-supervised [59]	1805:1857	10 fold	5	-	-	62.4	-
MobileNetV2-SVM [41]	1805:1857	-	5	72.0	<u>74.8</u>	85.0	92.0
HOG-CNN	1805:1857	80:20	5	86.0	78.6	83.2	94.2

6. Discussion

This study comprehensively evaluated the proposed HOG-CNN model across three major retinal disease diagnosis tasks Age-related Macular Degeneration (AMD), Diabetic Retinopathy (DR), and Glaucoma demonstrating consistently competitive performance against state-of-the-art baselines. For AMD detection on the IC-AMD dataset, the proposed model achieved an accuracy, precision, and recall of 92.8%, along with an AUC of 94.5%, outperforming most existing methods. While S2C2L [55] attained a slightly higher AUC of 97.5%, our model offers a more balanced performance across all metrics, demonstrating robust and consistent classification capability. In DR detection using the APTOS 2019 dataset, HOG-CNN delivered outstanding results across both binary and multi-class settings. It outperformed competing models in binary classification with 98.5% precision, recall, and accuracy, and a leading AUC of 99.2%. In the multiclass task, it maintained high performance (83.2% accuracy, 94.2% AUC), demonstrating reliability for more gran-

Table 5: Accuracy results for Glaucoma diagnosis.

ORIGA Dataset (Glaucoma)							
Method	Nor:Abn	Train:Test	Class	Sen	Spec	Acc	AUC
EAMNet [44]	482:168	2 fold CV	2	-	-	-	88.0
SVM-SMOTE [46]	482:168	10 fold CV	2	87.6	77.9	82.8	88.9
18-CNN [45]	482:168	70:30	2	58.1	92.4	78.3	-
NasNet [60]	482:168	70:30	2	78.7	91.1	87.9	-
CNN-SVM [47]	660:453	70:30	2	89.5	100	95.6	-
ODGNet [43]	482:168	pretrained	2	<u>94.8</u>	<u>94.9</u>	<u>95.8</u>	97.9
CAD[42]	482:168	10 fold CV	2	98.10	93.3	96.50	<u>94.2</u>
HOG-CNN	482:168	80:20	2	83.9	82.0	83.9	87.2

ular DR grading. These results emphasize the model’s strong discriminative power and adaptability across varied classification challenges.

In glaucoma detection using the ORIGA dataset, HOG-CNN achieved an accuracy of 83.9%, sensitivity of 83.9%, specificity of 82.0%, and an AUC of 87.2%. While it did not surpass ensemble or segmentation-heavy models like CAD [42] or ODGNet [43], its performance remains competitive, especially given its simplicity and efficiency. Notably, the model requires no domain-specific pretraining or segmentation, offering a practical advantage in low-resource settings. Overall, the integration of handcrafted HOG features with CNN-based deep representations enables a lightweight yet powerful framework, capable of capturing both fine-grained textures and high-level semantics. These findings validate the HOG-CNN as a generalizable and interpretable tool for retinal disease screening in real-world clinical applications.

7. Limitations

Although the proposed HOG-CNN framework delivers state-of-the-art or near-state-of-the-art results across AMD, DR, and glaucoma benchmarks, its reliance on handcrafted HOG descriptors makes performance sensitive to image resolution and illumination, limits the value of standard geometric data augmentation, and may exclude richer, fully learnable representations; moreover, the off-the-shelf CNN backbone is not fine-tuned to the ophthalmic domain, and evaluation on the small ORIGA dataset constrains the generalisability of glaucoma findings, highlighting the need for larger, heterogeneous datasets and task-specific end-to-end training in future work.

8. Conclusion

This study introduces a hybrid HOG-CNN framework for retinal disease diagnosis, achieving strong and

consistent results across AMD, DR, and glaucoma classification tasks. By fusing handcrafted Histogram of Oriented Gradients (HOG) features with deep convolutional representations, the model captures both fine-grained texture and high-level semantic information. On the IC-AMD dataset, the proposed model achieved an accuracy of 92.8% and an AUC of 94.5%, surpassing several state-of-the-art methods in overall performance. In binary DR detection using the APTOS 2019 dataset, it attained 98.5% accuracy and 99.2% AUC, surpassing leading models such as SCL and C-DNN. For multiclass DR classification, it delivered 83.2% accuracy and the highest AUC of 94.2%, indicating robust performance in nuanced clinical grading. While performance on the ORIGA dataset for glaucoma (83.9% accuracy, 87.2% AUC) was slightly below the top-performing models, the HOG-CNN still demonstrated competitive results given its simplicity and lack of specialized preprocessing.

The model’s lightweight and interpretable architecture makes it well-suited for deployment in real-world, resource-limited settings. Its ability to outperform or match more complex models—without requiring extensive augmentation, segmentation, or transfer learning—underscores the value of integrating handcrafted and learned features. These findings highlight HOG-CNN as a practical and generalizable approach for automated retinal disease screening and a promising foundation for future clinical decision support systems.

9. Future Work

Future work will focus on fine-tuning the CNN backbone with domain-specific data, integrating more expressive topological features beyond HOG, and developing robust normalization methods to handle resolution and illumination variability. Expanding evaluation to larger, diverse datasets and real-world clinical settings is also essential. Additionally, incorporating interpretability tools tailored to hybrid models can enhance transparency and support clinical adoption.

Declarations

Funding

The author received no financial support for the research, authorship, or publication of this work.

Acknowledgement

The authors utilized an online platform to check and correct grammatical errors and to improve sentence readability.

Conflict of interest/Competing interests

The authors declare no conflict of interest.

Ethics approval and consent to participate

Not applicable. This study did not involve human participants or animals, and publicly available datasets were used.

Consent for publication

Not applicable.

Data availability

The datasets used in this study are publicly available. The APTOS 2019 dataset is accessible at <https://www.kaggle.com/c/aptos2019-blindness-detection>, and the IChallenge-AMD dataset was provided for the ADAM challenge as part of ISBI 2020.

Materials availability

Not applicable.

Code availability

The source code used in this study is publicly available at <https://github.com/FaisalAhmed77/HOG-CNN>.

Author’s Contribution

FA conceptualized the study, downloaded the data, prepared the code, performed the data analysis and wrote the manuscript. FA reviewed and approved the final version of the manuscript.

10. APPENDIX

Below, we provide additional performance metrics for our HOG-CNN model, utilizing various pre-trained CNN models as backbones.

Table .6: Accuracy results for HOG-CNN on APTOS dataset.

APTOS 2019 Dataset (DR) - Binary				
Method	Acc	Prec	Rec	AUC
Resnet50	96.73	96.73	96.73	98.28
HOG + Resnet50	98.09	97.96	98.09	98.54
DenseNet201	96.55	96.72	96.55	97.81
HOG + DenseNet201	96.45	96.45	96.45	98.14
InceptionResNetV2	52.91	52.91	52.91	52.91
HOG + InceptionResNetV2	94.54	94.54	94.41	94.72
MobileNetV2	94.73	94.73	94.73	96.72
HOG + MobileNetV2	95.50	95.37	95.50	97.03
EfficientNetB3	96.91	97.09	96.91	98.68
HOG + EfficientNetB3	98.50	98.47	98.50	99.21
Xception	94.73	94.74	94.91	97.47
HOG + Xception	94.68	94.68	94.68	93.03
VGG19	96.91	96.91	96.91	97.80
HOG + VGG19	96.18	96.31	96.04	97.97
InceptionV3	91.64	91.64	91.64	95.87
HOG + InceptionV3	95.36	95.36	95.36	95.85
EfficientNetB0	97.64	97.64	97.64	98.62
HOG + EfficientNetB0	98.36	98.36	98.36	98.86
EfficientNetB2	96.91	96.90	96.73	98.28
HOG + EfficientNetB2	98.36	98.36	98.36	98.94

Table .7: Accuracy results for our HOG-CNN models on APTOS dataset (5-labels) with different backbones.

APTOS 2019 Dataset (DR) for 5-class				
Method	Acc	Prec	Rec	AUC
Resnet50	76.73	77.67	75.27	90.54
HOG + Resnet50	78.99	83.36	72.44	89.43
DenseNet201	74.36	75.83	70.18	90.81
HOG + DenseNet201	73.64	78.98	70.36	92.53
MobileNetV2	71.27	73.00	69.82	88.80
HOG + MobileNetV2	78.17	78.61	77.22	80.89
EfficientNetB3	76.00	76.74	74.36	92.85
HOG + EfficientNetB3	82.26	86.32	77.49	93.66
Xception	71.09	77.63	64.36	91.00
HOG + Xception	79.13	82.15	74.08	88.80
VGG19	78.55	86.73	71.27	95.65
HOG + VGG19	79.67	84.03	71.76	92.26
InceptionV3	69.45	69.91	68.00	89.09
HOG + InceptionV3	77.49	78.04	76.13	82.41
EfficientNetB0	78.55	78.83	78.55	92.34
HOG + EfficientNetB0	83.49	84.09	82.95	88.70
EfficientNetB2	78.55	79.81	76.91	94.25
HOG + EfficientNetB2	83.22	85.97	78.58	94.15

Table .8: Accuracy results for our HOG-CNN models on IChallenge dataset with different backbones.

IChallenge Dataset (AMD)				
Method	Acc	Prec	Rec	AUC
Resnet50	87.34	87.34	87.34	86.54
HOG + Resnet50	91.75	86.56	76.27	92.01
DenseNet201	78.48	79.49	78.48	88.05
HOG + DenseNet201	89.50	80.38	70.92	89.78
InceptionResNetV2	21.52	21.52	21.52	50.00
HOG + InceptionResNetV2	87.50	87.34	86.25	89.14
MobileNetV2	86.08	85.90	84.81	91.67
HOG + MobileNetV2	90.00	88.89	90.00	92.23
EfficientNetB3	88.61	88.75	89.87	95.95
HOG + EfficientNetB3	92.75	88.71	77.52	93.61
Xception	84.81	84.81	84.81	88.24
HOG + Xception	86.25	87.84	81.25	91.11
VGG19	86.08	86.08	86.08	92.31
HOG + VGG19	90.00	88.89	90.00	90.95
InceptionV3	72.15	72.15	72.15	82.73
HOG + InceptionV3	87.50	87.34	86.25	89.66
EfficientNetB0	86.08	85.00	86.08	90.12
HOG + EfficientNetB0	92.75	90.07	76.41	93.13
EfficientNetB2	87.34	87.34	87.34	90.24
HOG + EfficientNetB2	92.75	94.82	71.96	94.49

Table .9: Accuracy results for our HOG-CNN models on ORIGA dataset with different backbones.

ORIGA Dataset (Glaucoma)				
Method	Acc	Prec	Rec	AUC
Resnet50	73.08	73.08	73.08	78.50
HOG + Resnet50	81.54	81.89	80.00	87.08
DenseNet201	68.46	67.72	66.15	75.90
HOG + DenseNet201	79.23	79.07	78.46	84.06
InceptionResNetV2	73.85	73.85	73.85	73.85
HOG + InceptionResNetV2	80.00	80.00	80.00	80.62
MobileNetV2	71.54	71.54	71.54	74.71
HOG + MobileNetV2	78.46	76.60	83.08	79.34
EfficientNetB3	73.85	74.05	74.62	82.46
HOG + EfficientNetB3	83.08	81.95	83.85	88.67
Xception	65.38	65.12	64.62	75.90
HOG + Xception	79.235	77.27	78.46	80.00
VGG19	69.23	68.94	70.00	76.41
HOG + VGG19	79.23	78.63	79.23	85.10
InceptionV3	75.38	75.59	73.85	82.88
HOG + InceptionV3	79.23	78.63	79.23	82.07
EfficientNetB0	70.00	70.00	70.00	77.95
HOG + EfficientNetB0	83.85	81.95	83.85	87.23
EfficientNetB2	64.62	65.89	65.38	67.74
HOG + EfficientNetB2	81.54	77.14	83.08	87.02

References

- [1] W. H. Organization, Blindness and vision impairment, 2023. URL: <https://www.who.int/news-room/fact-sheets/detail/blindness-and-visual-impairment>, accessed: 2025-05-02.
- [2] P. S. Silva, D. Zhang, C. M. P. Jacoba, W. Fickweiler, D. Lewis, J. Leitmeyer, K. Curran, R. P. Salongcay, D. Doan, M. Ashraf, et al., Automated machine learning for predicting diabetic retinopathy progression from ultra-widefield retinal images, *JAMA ophthalmology* 142 (2024) 171–178.
- [3] E. R. Dow, H. K. Jeong, E. A. Katz, C. A. Toth, D. Wang, T. Lee, D. Kuo, M. J. Allingham, M. Hadziahmetovic, P. S. Mettu, et al., A deep-learning algorithm to predict short-term progression to geographic atrophy on spectral-domain optical coherence tomography, *JAMA ophthalmology* 141 (2023) 1052–1061.
- [4] T. Li, W. Bo, C. Hu, H. Kang, H. Liu, K. Wang, H. Fu, Applications of deep learning in fundus images: A review, *Medical Image Analysis* 69 (2021) 101971.
- [5] D. S. Ting, et al., Deep learning in ophthalmology: the technical and clinical considerations, *Progress in retinal and eye research* 72 (2019) 100759.
- [6] M. H. Sarhan, et al., Machine learning techniques for ophthalmic data processing: a review, *IEEE Journal of Biomedical and Health Informatics* 24 (2020) 3338–3350.
- [7] D. S. W. Ting, et al., Artificial intelligence and deep learning in ophthalmology, *British Journal of Ophthalmology* 103 (2019) 167–175.
- [8] N. Dalal, B. Triggs, Histograms of oriented gradients for human detection, in: 2005 IEEE computer society conference on computer vision and pattern recognition (CVPR'05), volume 1, Ieee, 2005, pp. 886–893.
- [9] A. Singh, S. Sengupta, V. Lakshminarayanan, Explainable deep learning models in medical image analysis, *Journal of imaging* 6 (2020) 52.
- [10] A. Fourcade, R. H. Khonsari, Deep learning in medical image analysis: A third eye for doctors, *Journal of stomatology, oral and maxillofacial surgery* 120 (2019) 279–288.
- [11] H. Pratt, F. Coenen, D. M. Broadbent, S. P. Harding, Y. Zheng, Convolutional neural networks for diabetic retinopathy, *Procedia computer science* 90 (2016) 200–205.
- [12] F. Ahmed, M. A. N. Bhuiyan, B. Coskunuzer, Topo-cnn: Retinal image analysis with topological deep learning, *Journal of Imaging Informatics in Medicine* (2025) 1–17.
- [13] F. Ahmed, B. Coskunuzer, Tofi-ml: Retinal image screening with topological machine learning, in: *Annual Conference on Medical Image Understanding and Analysis*, Springer, 2023, pp. 281–297.
- [14] F. Ahmed, Topological Machine Learning in Medical Image Analysis, Ph.D. thesis, The University of Texas at Dallas, 2023.
- [15] T. Qaiser, Y.-W. Tsang, D. Taniyama, N. Sakamoto, K. Nakane, D. Epstein, N. Rajpoot, Fast and accurate tumor segmentation of histology images using persistent homology and deep convolutional features, *Medical image analysis* 55 (2019) 1–14.
- [16] P. Lawson, A. B. Sholl, J. Q. Brown, B. T. Fasy, C. Wenk, Persistent homology for the quantitative evaluation of architectural features in prostate cancer histology, *Scientific reports* 9 (2019) 1139.
- [17] A. Yadav, F. Ahmed, O. Daescu, R. Gedik, B. Coskunuzer, Histopathological cancer detection with topological signatures, in: 2023 IEEE International Conference on Bioinformatics and Biomedicine (BIBM), 2023, pp. 1610–1619. doi:10.1109/BIBM58861.2023.10385822.
- [18] E. Berry, Y.-C. Chen, J. Cisewski-Kehe, B. T. Fasy, Functional summaries of persistence diagrams, *Journal of Applied and Computational Topology* 4 (2020) 211–262.
- [19] L. Crawford, et. al., Predicting clinical outcomes in glioblastoma: an application of topological and functional data analysis, *J.Amer.Stat.Assoc.* 115 (2020) 1139–1150.
- [20] A. Yadav, F. Ahmed, O. Daescu, R. Gedik, B. Coskunuzer, Histopathological cancer detection with topological signatures, in: 2023 IEEE International Conference on Bioinformatics and Biomedicine (BIBM), IEEE, 2023, pp. 1610–1619.
- [21] F. Ahmed, B. Nuwagira, F. Torlak, B. Coskunuzer, Topo-CXR: Chest X-ray TB and Pneumonia Screening with Topological Machine Learning, in: *Proceedings of the IEEE/CVF International Conference on Computer Vision*, 2023, pp. 2326–2336.
- [22] L. Kanari, et al., A topological representation of branching neuronal morphologies, *Neuroinformatics* 16 (2018) 3–13.
- [23] P. Bendich, J. S. Marron, E. Miller, A. Pieloch, S. Skwerer, Persistent homology analysis of brain artery trees, *The annals of applied statistics* 10 (2016) 198.
- [24] B. Rieck, et al., Uncovering the topology of time-varying fmri data using cubical persistence, *NeurIPS* 33 (2020) 6900–6912.
- [25] B. J. Stolz, et al., Topological data analysis of task-based fmri data from experiments on schizophrenia, *Journal of Physics: Complexity* 2 (2021) 035006.
- [26] P. G. Cámara, A. J. Levine, R. Rabadan, Inference of ancestral recombination graphs through topological data analysis, *PLoS computational biology* 12 (2016) e1005071.
- [27] J. I. Orlando, et al., An ensemble deep learning based approach for red lesion detection in fundus images, *Computer methods and programs in biomedicine* 153 (2018) 115–127.
- [28] A. You, J. K. Kim, I. H. Ryu, T. K. Yoo, Application of generative adversarial networks (gan) for ophthalmology image domains: a survey, *Eye and Vision* 9 (2022) 1–19.
- [29] O. Srivastava, et al., Artificial intelligence and machine learning in ophthalmology: A review, *Indian Journal of Ophthalmology* 71 (2023) 11–17.
- [30] N. D. Koseoglu, T. Liu, Predictive deep learning applications in ophthalmology, *Rev. Ophthalmol* 17 (2023).
- [31] M. Ashtari-Majlan, M. M. Dehshibi, D. Masip, Glaucoma diagnosis in the era of deep learning: A survey, *Expert Systems with Applications* 256 (2024) 124888.
- [32] D. M. Nguyen, H. M. T. Alam, T. Nguyen, D. Srivastav, H.-J. Profitlich, N. Le, D. Sonntag, Deep learning for ophthalmology: The state-of-the-art and future trends, *arXiv preprint arXiv:2501.04073* (2025).
- [33] H. Fang, et al., ADAM challenge: Detecting age-related macular degeneration from fundus images, *IEEE Transactions on Medical Imaging* (2022).
- [34] H. Fu, et al., ADAM: Automatic detection challenge on AMD, 2020. doi:10.21227/dt4f-rt59.
- [35] Z. Zhang, et al., Origa-light: An online retinal fundus image database for glaucoma analysis and research, in: 2010 Annual international conference of the IEEE engineering in medicine and biology, IEEE, 2010, pp. 3065–3068.
- [36] APTOS, Asia Pacific Tele-Ophthalmology Society (APTOS) 2019 Blindness Detection Dataset, 2019. <https://www.kaggle.com/c/aptos2019-blindness-detection>.
- [37] B. Goutam, M. F. Hashmi, Z. W. Geem, N. D. Bokde, A comprehensive review of deep learning strategies in retinal disease diagnosis using fundus images, *IEEE Access* (2022).
- [38] M. R. Islam, et al., Applying supervised contrastive learning for the detection of DR and its severity levels from fundus images, *Computers in Biology and Medicine* 146 (2022) 105602.
- [39] J. D. Bodapati, et al., Composite deep neural network with gated-attention mechanism for DR severity classification, *J.*

- Amb. Int. Hum. Compt. 12 (2021) 9825–9839.
- [40] P. Macsik, J. Pavlovicova, J. Goga, S. Kajan, Local binary cnn for diabetic retinopathy classification on fundus images, *Acta Polytech. Hung.* 19 (2022) 27–45.
 - [41] A. R. Singh, G. Singh, N. Saluja, L. Garg, Mobilenetv2-svm hybrid model classification of diabetic retinopathy effected human eye, in: 2024 Global Conference on Communications and Information Technologies (GCCIT), IEEE, 2024, pp. 1–5.
 - [42] L. K. Singh, M. Khanna, H. Garg, R. Singh, M. Iqbal, A three-stage novel framework for efficient and automatic glaucoma classification from retinal fundus images, *Multimedia Tools and Applications* 83 (2024) 85421–85481.
 - [43] J. Latif, S. Tu, C. Xiao, S. Ur Rehman, A. Imran, Y. Latif, Odgnet: a deep learning model for automated optic disc localization and glaucoma classification using fundus images, *SN Applied Sciences* 4 (2022) 1–11.
 - [44] W. Liao, et al., Clinical interpretable deep learning model for glaucoma diagnosis, *IEEE journal of biomedical and health informatics* 24 (2019) 1405–1412.
 - [45] P. Elangovan, M. K. Nath, Glaucoma assessment from color fundus images using convolutional neural network, *Int. J. of Imaging Systems and Technology* 31 (2021) 955–971.
 - [46] X. Zhao, F. Guo, Y. Mai, J. Tang, X. Duan, B. Zou, L. Jiang, Glaucoma screening pipeline based on clinical measurements and hidden features, *IET Image Processing* 13 (2019) 2213–2223.
 - [47] S. Ajitha, J. D. Akkara, M. Judy, Identification of glaucoma from fundus images using deep learning techniques, *Indian Journal of Ophthalmology* 69 (2021) 2702.
 - [48] Z. Wu, Y. Xiong, S. X. Yu, D. Lin, Unsupervised feature learning via non-parametric instance discrimination, in: *CVPR*, 2018, pp. 3733–3742.
 - [49] M. Ye, X. Zhang, P. C. Yuen, S.-F. Chang, Unsupervised embedding learning via invariant and spreading instance feature, in: *CVPR*, 2019, pp. 6210–6219.
 - [50] Z. Feng, C. Xu, D. Tao, Self-supervised representation learning by rotation feature decoupling, in: *CVPR*, 2019, pp. 10364–10374.
 - [51] T. Chen, S. Kornblith, M. Norouzi, G. Hinton, A simple framework for contrastive learning of visual representations, in: *ICML*, PMLR, 2020, pp. 1597–1607.
 - [52] X. Li, X. Hu, X. Qi, L. Yu, W. Zhao, P.-A. Heng, L. Xing, Rotation-oriented collaborative self-supervised learning for retinal disease diagnosis, *IEEE Transactions on Medical Imaging* 40 (2021) 2284–2294.
 - [53] Z. Zhang, Z. Ji, Q. Chen, S. Yuan, W. Fan, Joint optimization of cyclegan and cnn classifier for detection and localization of retinal pathologies on color fundus photographs, *IEEE Journal of Biomedical and Health Informatics* 26 (2021) 115–126.
 - [54] R. Chakraborty, ., A. Pramanik, Dcnn-based prediction model for detection of AMD from color fundus images, *Medical & Bio. Eng. & Comp.* 60 (2022) 1431–1448.
 - [55] Q. Bi, H. Zheng, X. Sun, J. Yi, W. Zhang, Y. Huang, Y. Li, Y. Zheng, Self-supervised cross-level consistency learning for fundus image classification, in: *ICASSP 2024-2024 IEEE International Conference on Acoustics, Speech and Signal Processing (ICASSP)*, IEEE, 2024, pp. 1781–1785.
 - [56] S. S. Chaturvedi, K. Gupta, V. Ninawe, P. S. Prasad, Automated diabetic retinopathy grading using deep convolutional neural network, *arXiv preprint arXiv:2004.06334* (2020).
 - [57] J. D. Bodapati, et. al., Blended multi-modal deep convnet features for diabetic retinopathy severity prediction, *Electronics* 9 (2020) 914.
 - [58] G. Kumar, S. Chatterjee, C. Chattopadhyay, Dristi: a hybrid deep neural network for diabetic retinopathy diagnosis, *Signal, Image and Video Processing* 15 (2021) 1679–1686.
 - [59] F. Long, H. Xiong, J. Sang, A classification method for diabetic retinopathy based on self-supervised learning, in: *International Conference on Intelligent Computing*, Springer, 2024, pp. 347–357.
 - [60] I. A. Taj, et al., An ensemble framework based on deep CNNs for glaucoma classification., *Mathematical Biosciences and Engineering* 18 (2021) 5321–5347.